

Periodic magnetization structures generated by transverse spin current in magnetic nanowires

Volodymyr P. Kravchuk,^{1,*} Oleksii M. Volkov,² Denis D. Sheka,² and Yuri Gaididei¹

¹*Bogolyubov Institute for Theoretical Physics, 03143 Kiev, Ukraine*

²*Taras Shevchenko National University of Kiev, 01601 Kiev, Ukraine*

(Received 25 February 2013; revised manuscript received 21 May 2013; published 5 June 2013)

The magnetization behavior of long nanowires with square cross section under the influence of strong perpendicular spin-polarized current is studied theoretically. The study is based on Landau-Lifshitz-Slonczewski phenomenology. Without the current the wire is magnetized uniformly along its axis. For small currents the wire magnetization remains uniform, but it inclines with respect to the wire axis within the plane perpendicular to the current direction. With increasing current the inclination angle increases up to the maximum value $\pi/4$. Further current increase leads either to saturation or to a stable periodic multidomain structure depending on the wire thickness. For thick wires a hysteresis is observed in the saturation process under the action of the current. All critical parameters of the current induced magnetization behavior are determined theoretically. The study is carried out both analytically and numerically using micromagnetic simulations.

DOI: [10.1103/PhysRevB.87.224402](https://doi.org/10.1103/PhysRevB.87.224402)

PACS number(s): 75.10.Hk, 75.40.Mg, 05.45.-a, 72.25.Ba

I. INTRODUCTION

The usage of spin-polarized current is a convenient way to control the magnetic structures in nanowires without applying the external magnetic fields; that enables increasing the density of arrays of nanoscale elements in purely current controlled devices.^{1,2} Usually, the current is passed along the magnetic wire, this is so-called current-in-plane (CIP) configuration. In this case the influence of the current on the dynamics of domain walls is widely studied both theoretically and experimentally, see reviews (Refs. 3–6).

In the last few years an interest in the current-perpendicular-to-the-plane (CPP) configuration of nanowires has appeared, e.g., it was shown theoretically⁷ that in the CPP case the velocity of the domain wall can be much higher than those for the CIP stripe configuration with similar applied current densities. The similar domain wall motion was recently observed experimentally,^{8,9} where the typical current densities were much smaller than the densities which are commonly used in the CIP configurations. It was also shown^{10,11} that the domain wall can move even faster for the time alternating current in the CPP wire structure.

In this work we consider the CPP nanowire configuration, see Fig. 1. We study possible stationary states and their stability under the action of spin-polarized current. We found that there exists a critical transverse size h_c of the nanowire. For sizes $h < h_c$ a stable periodic domain structure appears in the presaturated regime; for thicker wires ($h > h_c$) the process of transverse saturation by current has a hysteresis, i.e., the critical current of transition to the saturated state (in the process of the current increasing) is larger than the critical current of the saturated state breaking (in the process of the current decreasing). Recently we reported on the formation of a stable periodic square vortex-antivortex lattice (vortex crystal) in the presaturated regime of the magnetic films of CPP configuration.^{12,13} The aim of this paper is to determine how the strong restriction of film size in one dimension affects the current-induced behavior of magnetization. In addition to the above-mentioned results we found that only stationary states take place in the nanowire with CPP geometry, contrary to films where the essentially dynamic regimes such as fluidlike

and gaslike dynamics of vortices and antivortices appear for current decreasing.^{12,13}

The paper is organized in the following way: In Sec. II we introduce a mathematical model of the one-dimensional magnetic nanowire which is based on the Landau-Lifshitz-Slonczewski equation. Here we adapt the spin operators representations of Holstein-Primakoff and Tyablikov for our classical system (Sec. II A). Considering the case of soft ferromagnet we take into account exchange and dipole-dipole interactions and derive the corresponding Hamiltonian in the wave-vector space (Sec. II B). In Sec. III we obtain two possible uniform stationary solutions and analyze their stability. The nonuniform stationary solution, the periodic domain structure, which arises as a result of instability of the saturates state, we study in Sec. IV. In whole, the magnetization behavior of the nanowire under the current influence is summarized in Sec. V, and the mathematical details of deriving an equation of motion and Hamiltonian are placed in Appendixes A and B.

II. ONE-DIMENSIONAL DISCRETE MODEL

We consider here a narrow nanowire of square cross section whose transverse size h is small enough to ensure one dimensionality of the magnetization, see Fig. 1. In other words we assume that the magnetization is varying only along the wire \hat{x} axis. This assumption works for the cases when h is comparable to or smaller than the characteristic magnetic length of the material, see Sec. II B. We assume that the total length of the wire $L \gg h$. The frame of reference is chosen as shown in Fig. 1. The magnetic media is modeled as a discrete¹⁴ cubic lattice of magnetic moments \mathbf{M}_v , where $v = a(v_x, v_y, v_z)$ is a three dimensional index with a being the lattice constant and $v_x, v_y, v_z \in \mathbb{Z}$. It is convenient to introduce the following notations: $N_x = L/a$ is the total number of lattice nodes along the \hat{x} -axis and $N_s = h^2/a^2$ is the number of nodes within the cross-section square.

We base our study on the classical one-dimensional discrete Landau-Lifshitz-Slonczewski equation:^{15–17}

$$\dot{\mathbf{m}}_n = \mathbf{m}_n \times \partial \mathcal{E} / \partial \mathbf{m}_n - \mathcal{J} \varepsilon_n \mathbf{m}_n \times [\mathbf{m}_n \times \hat{\mathbf{z}}], \quad (1)$$

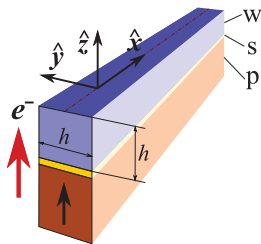


FIG. 1. (Color online) Geometry and notations of the problem. A long nanowire (w) is under the influence of the transversal spin-polarized current. The electrons gain the spin polarization while flowing through a ferromagnetic polarizer (p). A thin nonmagnetic spacer (s) is placed between the polarizer and the sample (wire). The cross section of the wire is assumed to be a square with a side h . The bold and thin arrows indicate the directions of conducting electron flow and the polarizer magnetization, respectively.

which describes the magnetization dynamics under the influence of spin-polarized current which flows perpendicular to the wire $\mathbf{J} = -J\hat{z}$ with $J > 0$, see Fig. 1. It is also assumed that the current flow and its spin polarization are of the same direction in Eq. (1). The index $n = av_x$ numerates the normalized magnetic moments $\mathbf{m}_n = \mathbf{M}_n/|\mathbf{M}_n|$ along the wire axis. The overdot indicates derivative with respect to the rescaled time in units of $(4\pi\gamma_0 M_s)^{-1}$, γ_0 is the gyromagnetic ratio, M_s is the saturation magnetization, and $\mathcal{E} = E/(4\pi M_s^2 a^3 \mathcal{N}_s)$ is dimensionless magnetic energy. The normalized electrical current density $\mathcal{J} = J/J_0$, where $J_0 = 4\pi M_s^2 |e| h / \hbar$ with e being electron charge and \hbar being Planck constant. The spin-transfer torque efficiency function ε_n has the form

$$\varepsilon_n = \frac{\eta}{(1 + \Lambda^{-2}) + (1 - \Lambda^{-2})m_n^z}, \quad (2)$$

where η is the degree of spin polarization and parameter $\Lambda \geq 1$ describes the mismatch between spacer and ferromagnetic resistance.^{17,18}

A. Holstein-Primakoff-Tyablikov representation

For the future analysis it is convenient to introduce a complex amplitude ψ_n of deviation from the stationary distribution of the magnetization (possible stationary states are considered below). For this purpose, we use a classical analog of Holstein-Primakoff representation¹⁹ for spin operators. Here we consider the general case of arbitrary form of the stationary state, where the magnetization distribution is determined by the unit vector

$$\boldsymbol{\gamma}_n = (\sin \Theta_n \cos \Phi_n, \sin \Theta_n \sin \Phi_n, \cos \Theta_n), \quad (3)$$

which can be index (coordinate) dependent. For this purpose, we also use the eigenrepresentation proposed by Tyablikov,²⁰ and finally, combining these two approaches, we obtain the following representation for the magnetization:

$$\mathbf{m}_n = \boldsymbol{\gamma}_n \frac{1 - |\psi_n|^2}{2} + \mathbf{A}_n \psi_n \sqrt{2 - |\psi_n|^2} + \text{c.c.}, \quad (4a)$$

where vector \mathbf{A}_n is orthogonal to $\boldsymbol{\gamma}_n$ and has the form

$$\mathbf{A}_n = \frac{1}{2}(\cos \Theta_n \cos \Phi_n + i \sin \Phi_n, \cos \Theta_n \sin \Phi_n - i \cos \Phi_n, -\sin \Theta_n). \quad (4b)$$

Using the representation (4) we obtain the following expressions for the magnetization components:

$$m_n^x + im_n^y = e^{i\Phi_n} \left\{ \sin \Theta_n (1 - |\psi_n|^2) + \sqrt{2 - |\psi_n|^2} \times \left[\psi_n \cos^2 \frac{\Theta_n}{2} - \psi_n^* \sin^2 \frac{\Theta_n}{2} \right] \right\}, \quad (5a)$$

$$m_n^z = \cos \Theta_n (1 - |\psi_n|^2) - \frac{\sin \Theta_n}{2} \sqrt{2 - |\psi_n|^2} (\psi_n + \psi_n^*). \quad (5b)$$

It should be noted that for the case of absence of deviations we have $\psi_n = 0$ and expressions (5) result in the magnetization orientated along the vector $\boldsymbol{\gamma}_n$. We used a similar procedure in Ref. 13 for the case of the uniform stationary state which is orientated along the current.

Substituting Eq. (5) into Eq. (1) enables one to proceed from the set of equations for the magnetization components to a single equation for the complex valued function ψ :

$$-i\dot{\psi}_n = \frac{\partial \mathcal{E}}{\partial \psi_n^*} + \mathcal{F}_n^{st}, \quad (6)$$

where the spin-torque term \mathcal{F}_n^{st} has the following form:

$$\mathcal{F}_n^{st} = i\mathcal{J}\varepsilon_n \left[\cos \Theta_n \psi_n \left(1 - \frac{1}{2}|\psi_n|^2 \right) + \sin \Theta_n \frac{1 - \frac{1}{4}(3 - |\psi_n|^2)(\psi_n^2 - |\psi_n|^2)}{\sqrt{2 - |\psi_n|^2}} \right]. \quad (7)$$

Here the efficiency function ε_n depends on ψ_n according to Eqs. (2) and (5b). For details of deriving Eq. (6) see Appendix A.

Since Eq. (6) describes the deviation from a stationary solution, it has a very convenient form for analysis of stability of the given stationary state. Although Eq. (6) can be used for an arbitrary stationary state, in what follows we restrict ourselves to the case of spatially uniform stationary states, so that $\Theta_n = \Theta = \text{const}$ and $\Phi_n = \Phi = \text{const}$. Here we study the linear stability, thus it is enough to use the linearized form of Eq. (6). It is also convenient to proceed to the wave-vector representation using the discrete Fourier transform

$$\psi_n = \frac{1}{\sqrt{\mathcal{N}_x}} \sum_k \hat{\psi}_k e^{ikn}, \quad (8a)$$

$$\hat{\psi}_k = \frac{1}{\sqrt{\mathcal{N}_x}} \sum_n \psi_n e^{-ikn}, \quad (8b)$$

with the orthogonality condition

$$\sum_n e^{i(k-k')n} = \mathcal{N}_x \Delta(k - k'), \quad (8c)$$

where $k = \frac{2\pi}{L}l$ is the two-dimensional discrete wave vector, $l \in \mathbb{Z}$, and $\Delta(k)$ is the Kronecker delta. Applying Eq. (8) to

the linearized equation (6) one gets the following equation of motion in the wave-vector space:

$$-i\dot{\hat{\psi}}_k = \frac{\partial \mathcal{E}^0}{\partial \hat{\psi}_k^*} + i\mathcal{J}\varepsilon^0 \left[\sqrt{\frac{\mathcal{N}_x}{2}} \sin \Theta + \cos \Theta \hat{\psi}_k + \frac{\varepsilon^0}{2\eta} (1 - \Lambda^{-2}) \sin^2 \Theta (\hat{\psi}_k + \hat{\psi}_{-k}^*) \right], \quad (9)$$

where $\varepsilon^0 = \eta / [(1 + \Lambda^{-2}) + (1 - \Lambda^{-2}) \cos \Theta]$ is the spin-transfer torque efficiency function (2) for the case $\psi_n = 0$ and \mathcal{E}^0 denotes the harmonic part of the normalized energy.

B. Hamiltonian of the system

We consider here the case of a soft ferromagnet, therefore we take into account only two contributions into the total energy: $E = E_{ex} + E_d$. Here

$$E_{ex} = -\mathcal{S}^2 \mathcal{J} \sum_{\mathbf{v}, \delta} \mathbf{m}_{\mathbf{v}} \cdot \mathbf{m}_{\mathbf{v}+\delta} \quad (10)$$

is the exchange contribution, where $\delta = a(\delta_x, \delta_y, \delta_z)$ is a three-dimensional index which numerates the nearest neighbors of an atom, value of spin is denoted with \mathcal{S} , and $\mathcal{J} > 0$ is the exchange integral between two nearest atoms.

The other term is the dipole-dipole energy

$$E_d = \frac{M_s^2 a^6}{2} \sum_{\mathbf{v} \neq \boldsymbol{\mu}} \left[\frac{(\mathbf{m}_{\mathbf{v}} \cdot \mathbf{m}_{\boldsymbol{\mu}})}{r_{\mathbf{v}\boldsymbol{\mu}}^3} - 3 \frac{(\mathbf{m}_{\mathbf{v}} \cdot \mathbf{r}_{\mathbf{v}\boldsymbol{\mu}})(\mathbf{m}_{\boldsymbol{\mu}} \cdot \mathbf{r}_{\mathbf{v}\boldsymbol{\mu}})}{r_{\mathbf{v}\boldsymbol{\mu}}^5} \right], \quad (11)$$

where we introduce the notation $\mathbf{r}_{\mathbf{v}\boldsymbol{\mu}} = (x_{\mathbf{v}\boldsymbol{\mu}}, y_{\mathbf{v}\boldsymbol{\mu}}, z_{\mathbf{v}\boldsymbol{\mu}}) = \boldsymbol{\mu} - \mathbf{v}$.

Hereinafter we will be interested only in the harmonic approximation \mathcal{E}^0 of the normalized energy which includes terms not higher than $\mathcal{O}(|\psi|^2)$. Thus

$$\mathcal{E}^0 = \mathcal{E}_{ex}^0 + \mathcal{E}_d^0, \quad (12)$$

where \mathcal{E}_{ex}^0 and \mathcal{E}_d^0 are harmonic parts of exchange and dipole-dipole energies, respectively. Substituting now the representation (5) to (10) and applying the Fourier transform (8), one obtains that the harmonic approximation of the normalized exchange energy reads

$$\mathcal{E}_{ex}^0 = \ell^2 \sum_k k^2 |\hat{\psi}_k|^2, \quad (13)$$

where the exchange length $\ell = \sqrt{\mathcal{S}^2 \mathcal{J} / (2\pi M_s^2 a)}$ determines the scale of magnetization inhomogeneities. Here we neglected possible surface effects which can arise due to the different number of nearest neighbors at the surface. The derivation of Eq. (13) is analogous to one presented in Appendix A1 of Ref. 13. The energy (13) coincides with the corresponding expression for the two-dimensional case obtained in Ref. 13. This is the direct consequence of the isotropic and local nature of the exchange interaction.

Let us proceed now to the dipole-dipole contribution. Since the magnetization depends only on the x coordinate, one can reduce the summation over all dimensions in Eq. (11) to the

summation over only the longitudinal dimension x :

$$E_d = \frac{M_s^2 a^6}{2} \sum_{\mathbf{v}_x, \boldsymbol{\mu}_x} \left[\sum_{\zeta=x,y,z} \mathcal{A}_{\mathbf{v}_x \boldsymbol{\mu}_x}^{\zeta} m_{\mathbf{v}_x}^{\zeta} m_{\boldsymbol{\mu}_x}^{\zeta} + \mathcal{B}_{\mathbf{v}_x \boldsymbol{\mu}_x} m_{\mathbf{v}_x}^y m_{\boldsymbol{\mu}_x}^z \right], \quad (14a)$$

where the summation over the transversal dimensions is enclosed in the coefficients

$$\mathcal{A}_{\mathbf{v}_x \boldsymbol{\mu}_x}^{\zeta} = \sum_{\substack{\bar{\mathbf{v}}, \bar{\boldsymbol{\mu}} \\ \mathbf{v} \neq \boldsymbol{\mu}}} \frac{r_{\bar{\mathbf{v}}\bar{\boldsymbol{\mu}}}^2 - 3\zeta_{\bar{\mathbf{v}}\bar{\boldsymbol{\mu}}}^2}{r_{\bar{\mathbf{v}}\bar{\boldsymbol{\mu}}}^5}, \quad \mathcal{B}_{\mathbf{v}_x \boldsymbol{\mu}_x} = -6 \sum_{\substack{\bar{\mathbf{v}}, \bar{\boldsymbol{\mu}} \\ \mathbf{v} \neq \boldsymbol{\mu}}} \frac{y_{\bar{\mathbf{v}}\bar{\boldsymbol{\mu}}} z_{\bar{\mathbf{v}}\bar{\boldsymbol{\mu}}}}{r_{\bar{\mathbf{v}}\bar{\boldsymbol{\mu}}}^5}. \quad (14b)$$

Here we introduced the notations $\bar{\mathbf{v}} = (v_x, v_y)$ and $\bar{\boldsymbol{\mu}} = (\mu_x, \mu_y)$ for the sake of simplicity. It is easy to show²¹ that $\mathcal{B}_{\mathbf{v}_x \boldsymbol{\mu}_x} \equiv 0$ for the case of rectangular wire cross section; the same is true for the cross sections in disk (cylindrical wire) or ring (tube) form. Substituting Eq. (5) into Eq. (14) and applying the Fourier transform (5), we obtain the following harmonic approximation for the normalized dipole-dipole energy (see Appendix B for details):

$$\begin{aligned} \mathcal{E}_d^0 = & - \sum_k \left\{ 3\sqrt{2\mathcal{N}_x} \sin \Theta g(0) \cos \Phi (\cos \Theta \cos \Phi \right. \\ & + i \sin \Phi) \hat{\psi}_k + \frac{3}{2} g(k) (\cos \Theta \cos \Phi + i \sin \Phi)^2 \hat{\psi}_k \hat{\psi}_{-k} \\ & \left. + \frac{1}{2} [g(k) + 2g(0)] (1 - 3 \sin^2 \Theta \cos^2 \Phi) |\hat{\psi}_k|^2 + \text{c.c.} \right\}, \end{aligned} \quad (15)$$

where the function $g(k)$ can be presented approximately as

$$g(k) \approx \frac{1}{2} \left[I_1 \left(\frac{kh}{\sqrt{\pi}} \right) K_1 \left(\frac{kh}{\sqrt{\pi}} \right) - \frac{1}{3} \right], \quad (16)$$

with $I_1(x)$ and $K_1(x)$ being modified Bessel functions of the first and second types, respectively. For the exact form of $g(k)$ and other details see Appendix B. Thus the transverse dimension h enters into the one-dimensional problem via the function g . This is a direct consequence of the nonlocal nature of the dipole-dipole interaction.

III. STATIONARY STATES OF THE SYSTEM

The stationary magnetization distribution is determined by Eq. (9) with $\dot{\hat{\psi}}_k \equiv 0$:

$$\left. \frac{\partial \mathcal{E}^0}{\partial \hat{\psi}_k^*} \right|_{\hat{\psi}_k=0} + \sin \Theta \frac{i\mathcal{J}\varepsilon^0 \sqrt{\mathcal{N}_x}}{\sqrt{2}} = 0. \quad (17)$$

Substitution of Eqs. (12), (13), and (15) into (17) results in the equation for stationary states of the system for a given value of the current \mathcal{J} :

$$\sin \Theta \left[i\mathcal{J}\varepsilon^0 - \frac{\cos \Phi}{2} (\cos \Theta \cos \Phi - i \sin \Phi) \right] = 0, \quad (18)$$

where we took into account that $g(0) = 1/12$.

There are two solutions of Eq. (18). The first one,

$$\sin \Theta = 0, \quad (19)$$

describes a saturated state when the wire is uniformly magnetized along the \hat{z} axis, i.e., along the current direction. The second solution of Eq. (18) reads

$$\begin{cases} \cos \Theta = 0, \\ \sin \Phi \cos \Phi = -\varkappa, \end{cases} \quad (20a)$$

$$\varkappa = \beta \frac{2\eta}{1 + \Lambda^{-2}}. \quad (20b)$$

In terms of magnetization components [Eq. (5)] the solution (20) has the following form:

$$m_n^z = 0, \quad (21a)$$

$$m_n^x(\varkappa) = \cos \Phi(\varkappa) = \left[\frac{1 + \sqrt{1 - 4\varkappa^2}}{2} \right]^{\frac{1}{2}}, \quad (21b)$$

$$m_n^y(\varkappa) = \sin \Phi(\varkappa) = - \left[\frac{1 - \sqrt{1 - 4\varkappa^2}}{2} \right]^{\frac{1}{2}} \approx -\varkappa. \quad (21c)$$

The solution (21) as well as (20) exists for the current interval $0 \leq \varkappa \leq 1/2$ that corresponds to the varying of the angle Φ in the interval $-\pi/4 \leq \Phi \leq 0$.

In the following we consider stability of each of the solutions (19) and (20). Let us start from the stability analysis of the solution (20). To obtain the equation of motion linearized in the vicinity of the stationary solution, we substitute Eq. (20) into Eqs. (9) and (12), resulting in

$$-i \dot{\hat{\psi}}_k = \frac{\partial \mathcal{E}^0}{\partial \hat{\psi}_k^*} + i \frac{\varkappa}{4} \frac{1 - \Lambda^{-2}}{1 + \Lambda^{-2}} (\hat{\psi}_k + \hat{\psi}_{-k}^*), \quad (22a)$$

$$\begin{aligned} \mathcal{E}^0 = & \sum_k \frac{3}{2} g(k) \sin^2 \Phi(\varkappa) (\hat{\psi}_k \hat{\psi}_{-k} + \hat{\psi}_k^* \hat{\psi}_{-k}^*) \\ & + |\hat{\psi}_k|^2 \{ \ell^2 k^2 + [g(k) + 2g(0)][2 - 3 \sin^2 \Phi(\varkappa)] \}, \end{aligned} \quad (22b)$$

where the function $\sin \Phi(\varkappa)$ is determined by Eq. (21c). The linear Eq. (22a) has the solution $\hat{\psi}_k^\pm = \Psi_\pm e^{z_\pm(k)t}$, where the rate function $z_\pm(k)$ is

$$z_\pm(k) = \frac{1}{2} [-\bar{\varkappa} \pm \sqrt{\bar{\varkappa}^2 - 4\alpha^+ \alpha^-}], \quad (23a)$$

with

$$\alpha^\pm(k) = \ell^2 k^2 + [g(k) + 2g(0)][2 - 3 \sin^2 \Phi(\varkappa)] \pm 3g(k) \sin^2 \Phi(\varkappa), \quad (23b)$$

$$\bar{\varkappa} = \frac{\varkappa}{2} \frac{1 - \Lambda^{-2}}{1 + \Lambda^{-2}}. \quad (23c)$$

In accordance with Eq. (23a) the normalized current $\bar{\varkappa}$ plays the role of an effective damping,²² that is why the natural damping can be omitted in the original equation (1). When

$$\alpha^+ \alpha^- < 0 \quad (24)$$

the rate z_\pm becomes positive, which results in instability of the stationary solution (20). Analysis of Eq. (23b) shows that for $h/\ell < \mathcal{C}_0$ with $\mathcal{C}_0 \approx 17.37$ the instability condition (24) is equivalent to the condition $\sin^2 \Phi > 1/2$. Thus for the considered interval $-\pi/4 \leq \Phi \leq 0$ or, in other words,

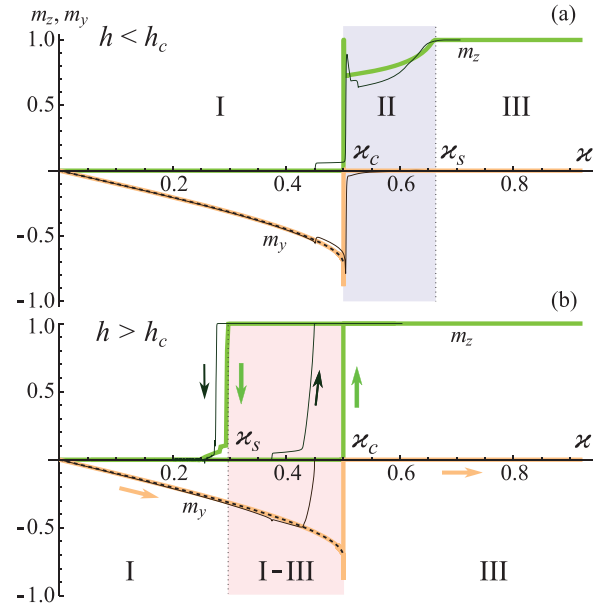


FIG. 2. (Color online) Components of the total magnetization of the nanowire as functions of the applied current density, which are normalized in accordance with Eq. (20b). Panels (a) and (b) correspond to wires with $h = 5$ nm and $h = 15$ nm, respectively. The results of micromagnetic simulations are shown by solid lines of different thicknesses: Thick curves correspond to the periodic boundary conditions along the \hat{x} axis, and the thin ones to the wire of finite length $L = 1 \mu\text{m}$. The analytical solution [Eq. (21c)] is shown by the dashed line.

for the current interval $0 \leq \varkappa \leq 1/2$ the stationary solution (20) is stable. We do not analyze the case of very thick nanowires because the assumption of one dimensionality of the magnetization does not work for the wire with thickness $h/\ell \gg 1$.

Thus, when the current is absent ($\varkappa = 0$) the wire is magnetized uniformly along its axis. Adiabatically slow increasing of the spin current from the value $\varkappa = 0$ to value $\varkappa = 1/2$ leads to the homogenous inclination of the wire magnetization by the angle $\Phi(\varkappa)$ which accordingly changes continuously from value $\Phi = 0$ to value $\Phi = -\pi/4$, where the function $\Phi(\varkappa)$ is determined by Eq. (20). The rotation takes place within the plane perpendicular to the current direction. The described regime takes place in region “I” and also in the hysteresis region “I-III” if the current is increasing, see Figs. 2 and 3. As one can see from the mentioned figures the analytically obtained behavior of the magnetization is in full agreement with micromagnetic simulations.²³ All simulations were performed for material parameters of permalloy: exchange constant $A = 1.3 \times 10^{-11}$ J/m, saturation magnetization $M_s = 8.6 \times 10^5$ A/m, and the anisotropy was neglected. The natural damping was also neglected $\alpha = 0$ by the reasons explained in the text. Rate of polarization $\eta = 0.4$ and $\Lambda = 2$ were fixed for all simulations.

The critical current $\varkappa_c = 1/2$ in physical units reads

$$J_c = \frac{\pi M_s^2 |e| h}{\hbar \eta} (1 + \Lambda^{-2}). \quad (25)$$

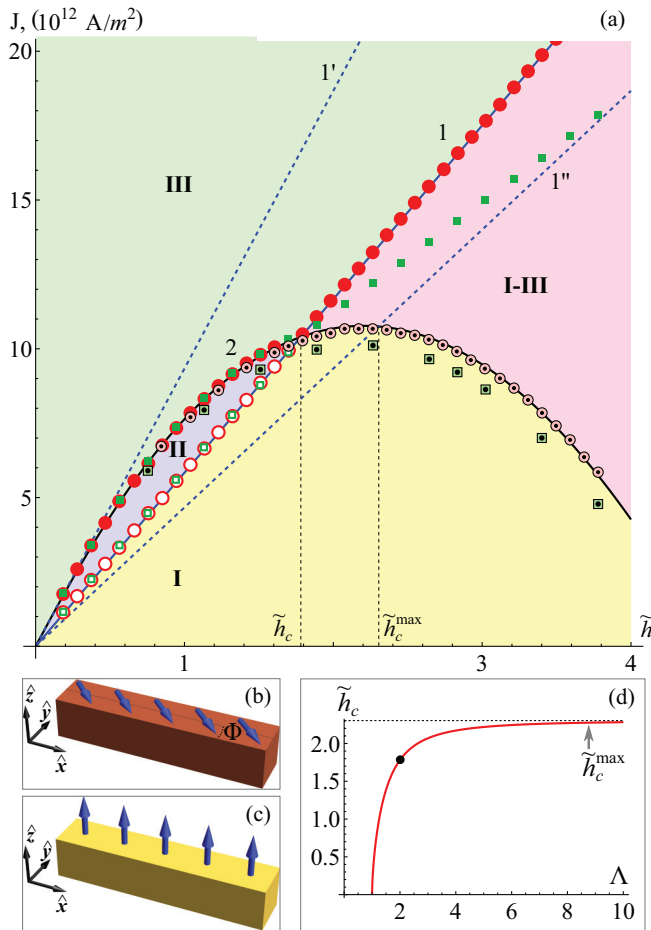


FIG. 3. (Color online) Diagram of stationary states of permalloy square nanowires with the transverse size $h = \tilde{h}\ell$ under spin-polarized current influence, panel (a). Panels (b) and (c) show the magnetization states for regions I and II respectively. Lines 1, 1', and 1'' represent the critical current (25) for the cases $\Lambda = 2$, $\Lambda = 1$, and $\Lambda \rightarrow \infty$, respectively. Line 2 shows the critical current (30). Crossing of the lines 1 and 2 determines the critical thickness \tilde{h}_c whose dependence on parameter Λ is shown in panel (d); the point shows the parameters of simulations: $\Lambda = 2$.

The dependence of the critical current J_c on the wire thickness h is a linear one with a slope which depends on the parameter Λ . The corresponding dependencies $J_c(h)$ are shown in Fig. 3(a) by lines 1, 1', and 1'' for different values of Λ .

IV. STABILITY OF THE SATURATED STATE. PERIODIC DOMAIN STRUCTURE

When the current overrides the value J_c the inclined uniform state [Eq. (20)] becomes unstable. The new stationary state, which occurs as a result of the instability, depends on the wire thickness h . If h exceeds some critical value h_c , which will be determined below, the nanowire very rapidly goes to the saturated regime where the magnetization is uniformly aligned along the \hat{z} axis. This behavior is demonstrated in Fig. 2(b). It should be noted that contrary to infinite wires (or closed wires) the transition to saturation for wires of finite length is not quite a sharp jump due to the transitional formations of saturated domains at the wire ends. For thin wires with thicknesses

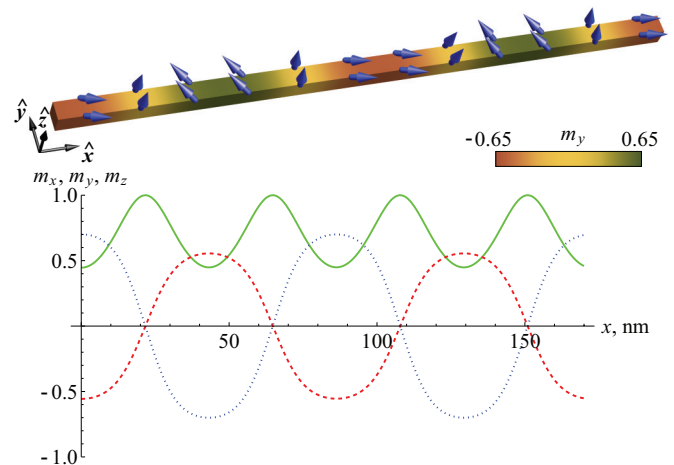


FIG. 4. (Color online) The domain structure which appears in nanowires with transverse size $h < h_c$. The data obtained using micromagnetic simulations. The 170 nm length part of a nanowire with thickness $h = 5$ nm and $L = 1$ μm is shown in the upper part of the figure. Magnetization distribution of the domain structure is shown by arrows and color scheme. Magnetization components along the wire are also plotted at the bottom: solid, dashed, and dotted lines correspond to m_z , m_y , and m_x , respectively.

$h < h_c$ the saturated state is unstable with respect to a periodic domain structure formation, see region “II” in Figs. 2 and 3. Magnetization distribution of the domain structure is shown in detail in Fig. 4. The stability of the domain structure was confirmed by micromagnetic simulations.

The described behavior of nanowires of different thicknesses under the spin-current action can be illustrated by the diagram of the stationary states, see Fig. 3. In region I the magnetization is spatially uniform, and it is inclined at the angle Φ in the plane perpendicular to the current direction, see Fig. 3(b). In region II a periodic domain structure appears, see Fig. 4. Region III corresponds to the saturated state, see Fig. 3(c). For wires with thickness $h > h_c$ the hysteresis region I-III arises, where the magnetization state coincides with the former state: either with the state I for the process of current increasing, or with the state III for the current decreasing from the saturation value. The corresponding hysteresis loop for component m_z is shown in Fig. 2(b). Boundaries between different stationary states shown on the diagram are obtained analytically. The positions of boundaries are verified by the micromagnetic simulations, whose results are shown by markers: Disks and squares represent the cases of the periodic boundary conditions and finite wire length $L = 1$ μm , respectively; open and filled markers correspond to transition from the inclined uniform state to the domain structure and to the saturated state, respectively, for the case of current increasing. Markers with dots show the currents when the saturated state becomes unstable for the case of the current decreasing.

To determine the critical thickness h_c and the saturation current for $h < h_c$ we consider the stability of the saturated state, when the quantization axis is directed along the \hat{z} axis. Substituting $\Theta = 0$ and $\Phi = 0$ ²⁴ into Eq. (15) enables us to

write the energy [Eq. (12)] of the system in the form

$$\mathcal{E}^0 = \sum_k \left\{ |\hat{\psi}_k|^2 [\ell^2 k^2 - g(k) - 2g(0)] - \frac{3}{2} g(k) (\hat{\psi}_k \hat{\psi}_{-k} + \hat{\psi}_k^* \hat{\psi}_{-k}^*) \right\} \quad (26)$$

and the equation of motion [Eq. (9)] in the form

$$-i \dot{\hat{\psi}}_k = \frac{\partial \mathcal{E}^0}{\partial \hat{\psi}_k^*} + i \tilde{\mathcal{J}} \hat{\psi}_k, \quad (27)$$

where $\tilde{\mathcal{J}} = \mathcal{J}\eta/2$. Since Eq. (27) is linear we will look for solutions in the form

$$\begin{aligned} \hat{\psi}_k &= \Psi_1^+ e^{\zeta_+(k)t} + \Psi_1^- e^{\zeta_-(k)t}, \\ \hat{\psi}_{-k}^* &= \Psi_2^+ e^{\zeta_+(k)t} + \Psi_2^- e^{\zeta_-(k)t}. \end{aligned} \quad (28)$$

In this case the rate function $\zeta_{\pm}(k)$ is

$$\zeta_{\pm}(k) = -\tilde{\mathcal{J}} \pm \tilde{\kappa}(k), \quad (29a)$$

$$\tilde{\kappa}(k) = \sqrt{9g^2(k) - [\ell^2 k^2 - g(k) - 2g(0)]^2}. \quad (29b)$$

As one can see from Eq. (29a) the current $\tilde{\mathcal{J}}$ plays the role of an effective damping as well as in case of the inclined solution (20). For $\tilde{\mathcal{J}} > \tilde{\kappa}(k)$ the rate function $\zeta_{\pm} < 0$ and it means that the saturated state is stable. However, for $\tilde{\mathcal{J}} < \max_k \tilde{\kappa}(k)$ the rate function becomes negative, $\zeta_+ < 0$, which means that the saturated state $\Theta = 0$ is linearly unstable. Thus, the minimum current at which the saturated state is stable can be obtained as $\tilde{\mathcal{J}}_s = \max_k \tilde{\kappa}(k)$ or equivalently in physical units

$$J_s = \frac{8\pi M_s^2 |e| h}{\hbar \eta} \max_k \tilde{\kappa}(k). \quad (30)$$

The dependence of the critical current [Eq. (30)] on the transverse wire size h is shown by line 2 in the diagram of states, see Fig. 3(a). The dependence $J_s(h)$ is not linear due to the dependence $\tilde{\kappa}(h)$, see Eqs. (29b) and (16).

It is important to note that the appearance of the periodic domain structure essentially depends on the resistance mismatch parameter Λ . Contrary to J_c the critical current J_s does not depend on the parameter Λ . Using Eqs. (16) and (29b), one can easily show that $\max_k \tilde{\kappa}(k) \rightarrow 3g(0) = 1/4$ for the case $h \rightarrow 0$. Comparing now Eqs. (30) and (25) we conclude that for $\Lambda = 1$ (minimal possible value) the line $J_c(h)$ is tangent to the curve $J_s(h)$ in point $h = 0$, see line 1' in Fig. 3(a). In this case $J_c(h) > J_s(h)$, and this means that the saturation, which appears when the current overrides the value J_c , remains stable and the domain structure is not formed. For the other case $\Lambda > 1$ the slope of the line $J_c(h)$ decreases and the intersection of the dependencies $J_c(h)$ and $J_s(h)$ determines the critical thickness h_c :

$$J_c(h_c) = J_s(h_c) \quad (31)$$

such that for $h < h_c$ the saturated state is unstable for currents $J < J_s$ and the stable periodic domain structure appears in the interval $J_c < J < J_s$.

For $h > h_c$ we have $J_c(h) > J_s(h)$ and a hysteresis takes place. When current increases from zero and reaches the critical value J_c the inclined uniform state (20) becomes

unstable and the system abruptly goes to the saturated state. By moving in the opposite direction, i.e., when we start to decrease current from the saturated state, it remains stable down to the current $J_s < J_c$. Note in passing that the transition from the saturated state to the inclined state (20) may be accompanied by the appearance of an irregular domain structure which arises due to degeneracy of the inclined state (20): If $\Phi = \Phi_0$ is one solution of Eq. (20), then $\Phi = \Phi_0 + \pi$ is another. The described hysteresis region is denoted ‘‘I-III’’ in Figs. 2(b) and 3(a).

Thus, under the adiabatic increase of the current the saturation value of the current depends on the wire thickness:

$$J_{\text{sat}} = \begin{cases} J_s, & \text{when } h < h_c, \\ J_c, & \text{when } h > h_c. \end{cases} \quad (32)$$

It is worth noting that for $h > h_c$ the saturation current for wires of finite length is slightly lower than J_c , see Fig. 3(a). This happens due to a particular role of the wire ends in the process of the saturation: For the currents $J \lesssim J_c$ domains magnetized along the \hat{z} axis occur at each of the ends. The length of the end domains rapidly increases with the current increasing and eventually the wire goes to the saturation state when the length of each of the domains reaches half of the wire length.

The critical thickness h_c determined by Eq. (31) depends on the parameter Λ , see Fig. 3(d). With Λ increasing the quantity h_c asymptotically approaches its maximum value $h_c^{\text{max}} \approx 2.303\ell$, see line 1'' in Fig. 3(a). For the minimal possible value $\Lambda = 1$ the critical thickness $h_c = 0$.

The above linear theory of instability of the saturated state enables us to determine the value of the saturation current. In order to calculate the domain structure which can appear just below the saturation one should carry out the nonlinear analysis. We do not provide it here, nevertheless we can estimate the period of the domain structure as $d \approx 2\pi/k_0$, where $k_0 = k_0(h)$ is a wave vector which maximizes function (29b): $\tilde{\kappa}(k_0) = \max_k \tilde{\kappa}(k)$. The critical thickness h_c separates two regimes of instability of the saturated state; the instability develops due to the softening of magnon modes with $k = k_0$ and $k = 0$ for cases $h < h_c$ and $h > h_c$, respectively.

V. CONCLUSIONS

We study theoretically the influence of perpendicular spin-polarized current on magnetization behavior of the long ferromagnetic nanowire of square cross section. We found out that under the action of current the magnetization of the wire always reaches some stationary state. This is in contrast to the case of planar films where either dynamical regimes or stationary states may realize for different current densities.^{12,13} Without the current the wire is uniformly magnetized along its axis. For current increasing within the interval $0 < J < J_c$ the wire magnetization remains spatially uniform being inclined in the plane perpendicular to the current direction. The inclination angle Φ depends on the current density J . The critical current J_c depends on the thickness and the mismatch parameter Λ . When the current overrides the value J_c the nanowire goes either to the saturated state where the magnetization is uniformly aligned along the direction of spin polarization of the current or to a periodic multidomain state, depending

on the wire thickness h . The domain structure exists for $h < h_c$ in the interval of currents $J_c < J < J_s$. In contrast to J_c the upper value of this interval J_s does not depend on the resistance mismatch parameter Λ . For thick wires with $h > h_c$ an opposite inequality $J_c > J_s$ holds and a hysteresis phenomenon takes place.

It should be noted that the strong saturation currents can complicate the experimental observation of the described effects. In order to overcome difficulties one can choose materials with low saturation magnetization, due to the scaling $J_{\text{sat}} \propto M_s^2$.

ACKNOWLEDGMENTS

The present work was partially supported by the Program of Fundamental Research of the Department of Physics and Astronomy of the National Academy of Sciences of Ukraine (Project No. 0112U000056).

APPENDIX A: EQUATION OF MOTION IN TERMS OF ψ FUNCTION

In accordance with Eq. (4) one can consider that $\mathbf{m}_n = \mathbf{m}_n(\psi, \psi^*)$. Projecting Eq. (1) to axes x and y , respectively, results in a set of equations

$$\begin{aligned} \frac{\partial m^x}{\partial \psi} \dot{\psi} + \frac{\partial m^x}{\partial \psi^*} \dot{\psi}^* &= m^y \frac{\partial \mathcal{E}}{\partial m^z} - m^z \frac{\partial \mathcal{E}}{\partial m^y} - j\epsilon m^x m^z, \\ \frac{\partial m^y}{\partial \psi} \dot{\psi} + \frac{\partial m^y}{\partial \psi^*} \dot{\psi}^* &= m^z \frac{\partial \mathcal{E}}{\partial m^x} - m^x \frac{\partial \mathcal{E}}{\partial m^z} - j\epsilon m^y m^z, \end{aligned} \quad (\text{A1})$$

where we omitted index n for the sake of simplicity. Solving the system (A1) with respect to $\dot{\psi}$ and $\dot{\psi}^*$ one obtains

$$\dot{\psi} = -\frac{m^z}{D} \left[\frac{\partial \mathcal{E}}{\partial \psi^*} + i\mathcal{F}^{st} \right], \quad (\text{A2a})$$

$$\mathcal{F}^{st} = -ij\epsilon \left(m^x \frac{\partial m^y}{\partial \psi^*} - m^y \frac{\partial m^x}{\partial \psi^*} \right). \quad (\text{A2b})$$

Here D is the determinant of (A1):

$$D = \frac{\partial m^x}{\partial \psi} \frac{\partial m^y}{\partial \psi^*} - \frac{\partial m^x}{\partial \psi^*} \frac{\partial m^y}{\partial \psi}. \quad (\text{A3})$$

Substituting Eq. (5) into Eq. (A3) results in $D = im^z$ and finally the equation (A2) takes the form of Eq. (6) with spin-torque term (7).

APPENDIX B: DIPOLE-DIPOLE CONTRIBUTION

Substituting Eq. (5) into Eq. (14), we obtain the harmonic part of the dipole-dipole energy in the wave-vector space in the form of

$$\begin{aligned} \mathcal{E}_d^0 &= - \sum_k \left\{ 3\sqrt{2\mathcal{N}_x} \sin \Theta \hat{\alpha}_0(0) \hat{\psi}_k + \frac{3}{2} \hat{\alpha}_1(k) \hat{\psi}_k \hat{\psi}_{-k} \right. \\ &\quad \left. + \frac{1}{2} |\hat{\psi}_k|^2 [\hat{\alpha}_2(k) + 2\hat{\alpha}_2(0)] + \text{c.c.} \right\}, \end{aligned} \quad (\text{B1})$$

where the coefficients $\hat{\alpha}_i(k)$ are

$$\begin{aligned} \hat{\alpha}_0(k) &= \frac{a^3}{8\pi \mathcal{N}_s} \sum_n \sum_{\bar{\nu}, \bar{\mu}} \frac{\cos \Theta (n^2 \cos^2 \Phi + y_{\nu\mu}^2 \sin^2 \Phi - z_{\nu\mu}^2) + i \sin \Phi \cos \Phi (n^2 - y_{\nu\mu}^2)}{(n^2 + y_{\nu\mu}^2 + z_{\nu\mu}^2)^{5/2}} e^{ikn}, \\ \hat{\alpha}_1(k) &= \frac{a^3}{8\pi \mathcal{N}_s} \sum_n \sum_{\bar{\nu}, \bar{\mu}} \frac{(n^2 - y_{\nu\mu}^2) (\cos 2\Phi + i \cos \Theta \sin 2\Phi) - \sin^2 \Theta (n^2 \cos^2 \Phi + y_{\nu\mu}^2 \sin^2 \Phi - z_{\nu\mu}^2)}{(n^2 + y_{\nu\mu}^2 + z_{\nu\mu}^2)^{5/2}} e^{ikn}, \\ \hat{\alpha}_2(k) &= \frac{a^3}{8\pi \mathcal{N}_s} \sum_n \sum_{\bar{\nu}, \bar{\mu}} \frac{n^2 + y_{\nu\mu}^2 - 2z_{\nu\mu}^2 - 3 \sin^2 \Theta (n^2 \cos^2 \Phi + y_{\nu\mu}^2 \sin^2 \Phi - z_{\nu\mu}^2)}{(n^2 + y_{\nu\mu}^2 + z_{\nu\mu}^2)^{5/2}} e^{ikn}. \end{aligned} \quad (\text{B2})$$

For the wires with cross sections in the form of square, disk, or ring, the indexes ν_y and ν_z are interchangeable, as well as indexes μ_y and μ_z . That enables us to simplify the expressions (B2) as

$$\begin{aligned} \hat{\alpha}_0(k) &= \cos \Phi (\cos \Theta \cos \Phi + i \sin \Phi) g(k), \\ \hat{\alpha}_1(k) &= (\cos 2\Phi - \sin^2 \Theta \cos^2 \Phi + i \cos \Theta \sin 2\Phi) g(k), \\ \hat{\alpha}_2(k) &= (1 - 3 \sin^2 \Theta \cos^2 \Phi) g(k), \end{aligned} \quad (\text{B3})$$

where the function $g(k)$ is

$$g(k) = \frac{a^3}{8\pi \mathcal{N}_s} \sum_n \sum_{\bar{\nu}, \bar{\mu}} \frac{n^2 - y_{\nu\mu}^2}{(n^2 + y_{\nu\mu}^2 + z_{\nu\mu}^2)^{5/2}} e^{ikn}. \quad (\text{B4})$$

To obtain a more suitable expression for the function $g(k)$ we proceed in Eq. (B4) from summation to integration. In this

case $g(k)$ can be presented as the sum of regular and singular parts in the following way:

$$g(k) = g_{\text{reg}}(k) + g_{\text{sing}}(k), \quad (\text{B5a})$$

$$\begin{aligned} g_{\text{reg}}(k) &= \frac{1}{\pi h^2} \lim_{r_0 \rightarrow 0} \int_{r_0}^{\infty} dx \cos(kx) \int_0^h dy \int_0^h dz \\ &\quad \times (h-y)(h-z) \frac{x^2 - y^2}{[x^2 + y^2 + z^2]^{5/2}}, \end{aligned} \quad (\text{B5b})$$

$$\begin{aligned} g_{\text{sing}}(k) &= \frac{1}{\pi h^2} \lim_{r_0 \rightarrow 0} \int_0^{r_0} dx \cos(kx) \int_0^{\pi/2} d\chi \int_{\sqrt{r_0^2 - x^2}}^{\sigma(x)} dr r \\ &\quad \times (h-r \sin \chi)(h-r \cos \chi) \frac{x^2 - r^2 \cos^2 \chi}{(x^2 + r^2)^{5/2}}. \end{aligned} \quad (\text{B5c})$$

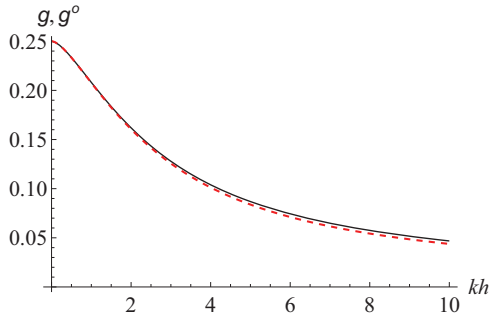


FIG. 5. (Color online) Comparison of regular parts of sum (B4) for wires with square and round cross sections. The solid and dashed lines correspond to the square and round wires, respectively, and represent expressions (B9) and (B12), respectively.

Here we used the relation

$$\int_0^h dy \int_0^h dy' F(|y - y'|) = 2 \int_0^h dy (h - y) F(y). \quad (\text{B6})$$

Furthermore in (B5c) we proceed to the polar frame of reference (r, χ) originated in one of the vertexes of the wire cross section, and the function $\sigma(\chi)$ determines the cross-section shape. In the following we will ascertain that the specific form of the function $\sigma(\chi)$ does not affect the value of the integral (B5c). To do this one should change the variables $r = r_0 \rho$, $x = r_0 \xi$ and find the limit in (B5c). The result is the following:

$$g_{\text{sing}}(k) = \frac{1}{\pi} \int_0^1 d\xi \int_0^{\pi/2} d\chi \int_{\sqrt{1-\xi^2}}^{\infty} d\rho \rho \frac{\xi^2 - \rho^2 \cos^2 \chi}{(\xi^2 + \rho^2)^{5/2}}. \quad (\text{B7})$$

The direct integration of Eq. (B7) results in

$$g_{\text{sing}}(k) = -\frac{1}{6}. \quad (\text{B8})$$

Let us now proceed to the calculation of the regular part [Eq. (B5b)]. The direct integration over variables y and z with the next integration by parts over x enables us to simplify

expression (B5b) as

$$g_{\text{reg}}(k) = \frac{1}{\pi kh} \int_0^{\infty} \sin(khx) \left(\frac{\sqrt{1+x^2}}{x} + \frac{x}{\sqrt{1+x^2}} - x \frac{\sqrt{2+x^2}}{1+x^2} - 1 \right) dx. \quad (\text{B9})$$

Using the representation (B9) one can easily obtain $g_{\text{reg}}(0) = 1/4$ and consequently

$$g(0) = \frac{1}{12}. \quad (\text{B10})$$

Let us consider the case $hk \ll 1$. In other words, the wire thickness is much smaller than the wavelength, meaning that the form of the wire cross section should not be of principle. To show this we calculate the regular part of function $g(k)$ for a nanowire with a disk-shaped cross section with radius $R = h/\sqrt{\pi}$, so the cross-section areas of round and square wires are equal. In this case the regular part of the sum (B4) can be presented by the integral

$$g_{\text{reg}}^o(k) = \frac{1}{4\pi h^2} \lim_{r_0 \rightarrow 0} \int_{r_0}^{\infty} dx \int_0^{2\pi} d\chi \int_0^{2\pi} d\chi' \int_0^{\frac{h}{\sqrt{\pi}}} dr \int_0^{\frac{h}{\sqrt{\pi}}} dr' \times \frac{rr' \cos(kx) [x^2 - (r \cos \chi - r' \cos \chi')^2]}{[x^2 + r^2 + r'^2 - 2rr' \cos(\chi - \chi')]^{5/2}}. \quad (\text{B11})$$

Using the parametrization

$$3 \frac{p^2}{(p^2 + c^2)^{5/2}} - \frac{1}{(p^2 + c^2)^{3/2}} = \int_0^{\infty} \xi^2 e^{-p\xi} J_0(c\xi) d\xi$$

and the relation

$$\int_0^{2\pi} J_0(\sqrt{r^2 + r'^2 - 2rr' \cos \chi}) = 2\pi J_0(r) J_0(r'),$$

where $J_0(x)$ is the Bessel function of the first kind, one can easily integrate the expression (B11) and obtain

$$g_{\text{reg}}^o(k) = \frac{1}{2} I_1 \left(\frac{kh}{\sqrt{\pi}} \right) K_1 \left(\frac{kh}{\sqrt{\pi}} \right), \quad (\text{B12})$$

where $I_1(x)$ and $K_1(x)$ are modified Bessel functions of the first and second kinds, respectively. Since the functions $g_{\text{reg}}(k)$ and $g_{\text{reg}}^o(k)$ are very close, see Fig. 5, one can use the approximation (16).

*vkravchuk@bitp.kiev.ua

¹S. S. P. Parkin, M. Hayashi, and L. Thomas, *Science* **320**, 190 (2008).

²D. A. Allwood, G. Xiong, C. C. Faulkner, D. Atkinson, D. Petit, and R. P. Cowburn, *Science* **309**, 1688 (2005).

³J. Lindner, *Superlattices Microstruct.* **47**, 497 (2010).

⁴G. Tatara, H. Kohno, and J. Shibata, *Phys. Rep.* **468**, 213 (2008).

⁵C. H. Marrows, *Adv. Phys.* **54**, 585 (2005).

⁶M. Kläui, *J. Phys.: Condens. Matter* **20**, 313001 (2008).

⁷A. V. Khvalkovskiy, K. A. Zvezdin, Y. V. Gorbunov, V. Cros, J. Grollier, A. Fert, and A. K. Zvezdin, *Phys. Rev. Lett.* **102**, 067206 (2009).

⁸C. T. Boone, J. A. Katine, M. Carey, J. R. Childress, X. Cheng, and I. N. Krivorotov, *Phys. Rev. Lett.* **104**, 097203 (2010).

⁹A. Chanthbouala, R. Matsumoto, J. Grollier, V. Cros, A. Anane, A. Fert, A. V. Khvalkovskiy, K. A. Zvezdin, K. Nishimura, Y. Nagamine, H. Maehara, K. Tsunekawa, A. Fukushima, and S. Yuasa, *Nat. Phys.* **7**, 626 (2011).

¹⁰P. Yan, Z. Z. Sun, J. Schliemann, and X. R. Wang, *Europhys. Lett.* **92**, 27004 (2010).

¹¹C. T. Boone and I. N. Krivorotov, *Phys. Rev. Lett.* **104**, 167205 (2010).

¹²O. M. Volkov, V. P. Kravchuk, D. D. Sheka, and Y. Gaididei, *Phys. Rev. B* **84**, 052404 (2011).

¹³Y. Gaididei, O. M. Volkov, V. P. Kravchuk, and D. D. Sheka, *Phys. Rev. B* **86**, 144401 (2012).

¹⁴The discrete model is used only for the sake of convenience of mathematical calculations; no discreteness effects are expected.

- ¹⁵J. C. Slonczewski, *J. Magn. Magn. Mater.* **159**, L1 (1996).
- ¹⁶L. Berger, *Phys. Rev. B* **54**, 9353 (1996).
- ¹⁷J. C. Slonczewski, *J. Magn. Magn. Mater.* **247**, 324 (2002).
- ¹⁸V. Sluka, A. Kákay, A. M. Deac, D. E. Bürgler, R. Hertel, and C. M. Schneider, *J. Phys. D: Appl. Phys.* **44**, 384002 (2011).
- ¹⁹T. Holstein and H. Primakoff, *Phys. Rev.* **58**, 1098 (1940).
- ²⁰S. V. Tyablikov, *Methods in the Quantum Theory of Magnetism*, 2nd ed. (Moscow, Nauka, 1975) [translation of 1st Russian ed. (Plenum Press, New York, 1967)].
- ²¹One should present \mathcal{B}_{v_x, μ_x} in integral form and perform the straightforward integration.
- ²²The effect of modifying the spin-wave attenuation by the Slonczewski spin torque in nanowires was also noted in X. J. Xing, Y. P. Yu, and S. W. Li, *Appl. Phys. Lett.* **95**, 142508 (2009).
- ²³We used the OOMMF code, version 1.2a5 (<http://math.nist.gov/oommf/>).
- ²⁴The angle Φ is not determined for the case $\Theta = 0$; we chose $\Phi = 0$ for convenience.